J. Fluid Mech. (1988), *vol.* 189, *pp.* 349–365
Printed in Great Britain

Characteristics of vorticity fluctuations in a turbulent wake

By R. A. ANTONIA, L. W. B. BROWNE AND D. A. SHAH
Department of Mechanical Engineering, University of Newcastle, NSW 2308, Australia

(Received 21 January 1987 and in revised form 9 September 1987)

Measurements of the lateral components of the vorticity fluctuation have been made in the self-preserving turbulent wake of a circular cylinder. Each component was obtained separately using two X-wires separated in the appropriate lateral directions. The two velocity derivatives which make up the streamwise vorticity component were also determined but not simultaneously. An approximation to the streamwise vorticity was made from these measurements. Moments, probability density functions and spectra of the three vorticity components across the wake are presented and discussed. The high-wavenumber behaviour of the spectra is compared with calculations, based on local isotropy. Satisfactory agreement with the calculations is obtained for the lateral vorticity components over a significant high-wavenumber range. The approximated streamwise vorticity spectrum tends towards the isotropic calculation at very large wavenumbers.

1. Introduction

Although vorticity is an important property of turbulent flows, relatively few characteristics for this quantity have been reported in the literature, presumably owing to the general difficulty of measurement. An indication of available measurements can be obtained from the surveys of Van Atta (1979), Willmarth (1979), Wallace & Vukoslavčević (1982) and Wallace (1986). Wallace surveys methods which employ arrays of hot-wire sensors as well as a range of other methods. The earlier measurements of the longitudinal vorticity were obtained with the Kovasznay (1950, 1955) four-wire probe. Using this probe, the spectrum of the longitudinal vorticity fluctuation was obtained by Kistler (1952) in grid turbulence while Corrsin & Kistler (1955) obtained r.m.s. values of the longitudinal vorticity across a boundary layer. Transverse vorticity measurements were reported by Eckelmann *et al.* (1977) who used a combination of single hot wire, an X-probe and a V-probe and by Foss (1979) who used an X-probe with parallel hot wires. More recently, Kastrinakis & Eckelmann (1983) used a modified version of the Kovasznay probe to measure the second-, third- and fourth-order moments of the longitudinal vorticity fluctuation in a fully developed turbulent channel flow. It would appear that simultaneous measurements of all three vorticity fluctuations can now be made with adequate accuracy. Such measurements were recently reported for a turbulent boundary layer by Balint, Vukoslavčević & Wallace (1987) using the miniature nine-sensor hot-wire probe.

The three components of the vorticity fluctuation ω_i are given, in Cartesian tensor notation, by

$$\omega_i = \epsilon_{ijk} \frac{\partial u_k}{\partial x_j}, \tag{1}$$

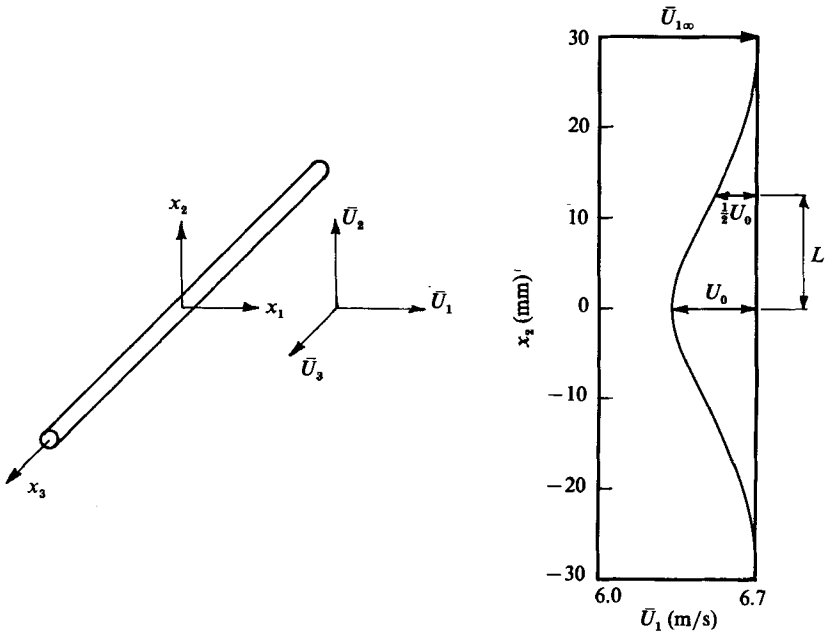

FIGURE 1. Definition sketch showing coordinate system and mean velocity profile.

where ϵ_{ijk} is the alternating tensor, equal to $+1$ if i,j,k are in cyclic order, equal to -1 if i,j,k are in anticyclic order and equal to zero if any two of the i,j,k are equal; and u_k is the velocity fluctuation in the x_k-direction.

The longitudinal vorticity component is thus

$$\omega_1 = \frac{\partial u_3}{\partial x_2} - \frac{\partial u_2}{\partial x_3} \equiv u_{3,2} - u_{2,3},$$

while the two lateral vorticity components are

$$\omega_2 = \frac{\partial u_1}{\partial x_3} - \frac{\partial u_3}{\partial x_1} \equiv u_{1,3} - u_{3,1},$$

and

$$\omega_3 = \frac{\partial u_2}{\partial x_1} - \frac{\partial u_1}{\partial x_2} \equiv u_{2,1} - u_{1,2}.$$

In a previous paper (Browne, Antonia & Shah 1987, hereinafter referred to as I), measurements were reported, in the self-preserving region of a turbulent wake, of nine of the velocity derivatives which feature in the turbulent-energy dissipation. Six of these derivatives were the velocity derivatives that appear in the three vorticity components. The derivatives $u_{1,3}$ and $u_{3,1}$ that make up ω_2 were obtained simultaneously from a pair of parallel X-wires separated in the x_3-direction, while the derivatives $u_{2,1}$ and $u_{1,2}$ that make up ω_3 were obtained simultaneously from a pair of parallel X-wires separated in the x_2-direction (the coordinate system is shown in figure 1). Although the derivatives $u_{3,2}$ and $u_{2,3}$ that make up ω_1 were also measured, they were not obtained simultaneously.

Although it now seems possible to determine the three components of ω_i simultaneously using a fixed-geometry multiple-wire vorticity probe (e.g. Wallace 1986), the measurements in I provided reasonably accurate, but non-simultaneous, estimates of all the velocity derivatives that feature in ω_i. These measurements

allowed reasonably accurate estimates of ω_2 and ω_3 as well as an approximation to ω_1 to be made. In this paper, we present statistics such as the probability density function (p.d.f.) and spectra of ω_2 and ω_3 and comment on the probable behaviour of corresponding statistics for ω_1. We also check the high-wavenumber behaviour of the ω_i spectra for local isotropy. Calculations of the one-dimensional spectra of ω_i, based on isotropy, are outlined in § 2. Experimental details are given in § 3 while the p.d.f. and associated moments of ω_i are discussed in § 4. Spectra of ω_i are presented in § 5 and a comparison between measured and calculated spectra is made in § 6.

2. Calculation of vorticity spectra based on local isotropy

For homogeneous turbulence, the fluctuating velocity and vorticity vectors can be expressed using a Fourier–Stieltjes representation (e.g. Batchelor 1953, p. 31)

$$u_i(\boldsymbol{x}) = \int_{-\infty}^{\infty} e^{i\boldsymbol{k}\cdot\boldsymbol{x}}\, dU_i(\boldsymbol{k}), \tag{2}$$

$$\omega_i(\boldsymbol{x}) = \int_{-\infty}^{\infty} e^{i\boldsymbol{k}\cdot\boldsymbol{x}}\, d\Omega_i(\boldsymbol{k}), \tag{3}$$

where $U_i(\boldsymbol{k})$ and $\Omega_i(\boldsymbol{k})$ are complex random functions with orthogonal increments $dU_i(\boldsymbol{k})$ and $d\Omega_i(\boldsymbol{k})$, $\boldsymbol{k}$ is the wavenumber vector and i, in the integrand, is $\sqrt{-1}$. The increments $dU_i(\boldsymbol{k})$ and $d\Omega_i(\boldsymbol{k})$ are related by

$$d\Omega_i(\boldsymbol{k}) = \epsilon_{ijk}\, ik_j\, dU_k(\boldsymbol{k}). \tag{4}$$

For homogeneous turbulence, the autocorrelation between vorticity vectors separated by $\boldsymbol{r}$ can be written as

$$\overline{\omega_i(\boldsymbol{x})\,\omega_j(\boldsymbol{x}+\boldsymbol{r})} = \int_{-\infty}^{\infty} e^{i\boldsymbol{k}\cdot\boldsymbol{r}}\, \psi_{ij}(\boldsymbol{k})\, d\boldsymbol{k}, \tag{5}$$

where $\psi_{ij}(\boldsymbol{k})$, the spectral density tensor, is given by

$$\psi_{ij}(\boldsymbol{k})\, d\boldsymbol{k} = \overline{d\Omega_i(\boldsymbol{k})\, d\Omega_j^*(\boldsymbol{k})}, \tag{6}$$

an asterisk denoting the complex conjugate. The one-dimensional power spectral density of ω_i is denoted by $\phi_{\omega_i}(k_1)$, defined so that

$$\int_{-\infty}^{\infty} \phi_{\omega_i}(k_1)\, dk_1 = \overline{\omega_i^2}, \tag{7}$$

where

$$\phi_{\omega_i}(k_1) = \int\int_{-\infty}^{\infty} \psi_{ii}(\boldsymbol{k})\, dk_2\, dk_3. \tag{8}$$

Using (4) and (6), it can be shown that (cf. Batchelor 1953, p. 39)

$$\psi_{ij}(\boldsymbol{k}) = (\delta_{ij}\, k^2 - k_i\, k_j)\, \phi_{ll}(\boldsymbol{k}) - k^2\, \phi_{ji}(\boldsymbol{k}), \tag{9}$$

where $\phi_{ij}(\boldsymbol{k})$ is the velocity spectral density tensor and δ_{ij} is the Kronecker delta, equal to one for $i = j$ and zero for $i \neq j$. The tensor $\phi_{ij}(\boldsymbol{k})$ is related to $dU_i(\boldsymbol{k})$ by the relation

$$\phi_{ij}(\boldsymbol{k})\, d\boldsymbol{k} = \overline{dU_i(\boldsymbol{k})\, dU_j^*(\boldsymbol{k})},$$

and satisfies the continuity equations

$$k_i\, \phi_{ij}(\boldsymbol{k}) = k_j\, \phi_{ij}(\boldsymbol{k}) = 0.$$

When isotropy is assumed, (9) reduces to

$$\psi_{ij}(\boldsymbol{k}) = \psi_{ij}(k) = k^2 \phi_{ij}(k), \tag{10}$$

with

$$\phi_{ij}(k) = \frac{E(k)}{4\pi k^4}(k^2 \delta_{ij} - k_i k_j), \tag{11}$$

where $E(k)$ is the three-dimensional spectrum and

$$\int_0^\infty E(k)\,\mathrm{d}k$$

is the total kinetic energy per unit mass.

Relatively simple expressions for $\phi_{\omega_i}(k_1)$ can be obtained using (10) and (11) in (8), transforming to polar coordinates and integrating over a plane orthogonal to the k_1-axis. Only the final results are written below:

$$\phi_{\omega_2}(k_1) = \phi_{\omega_3}(k_1) = \tfrac{1}{2}k_1^2 \int_{k_1}^\infty \frac{E(k)}{k}\,\mathrm{d}k + \frac{1}{4}\int_{k_1}^\infty \frac{E(k)}{k}(k^2 - k_1^2)\,\mathrm{d}k, \tag{12}$$

and

$$\phi_{\omega_1}(k_1) = \frac{1}{2}\int_{k_1}^\infty \frac{E(k)}{k}(k^2 - k_1^2)\,\mathrm{d}k. \tag{13}$$

The equality between ϕ_{ω_2} and ϕ_{ω_3} can be deduced from the equality between ψ_{22} and ψ_{33} and relations (8), (10) and (11). The isotropic spectrum of ω_1 differs from the isotropic spectra of ω_2 and ω_3, (13) indicating that ϕ_{ω_1} is equal to twice the second term on the right-hand side of (12).

3. Experimental details

Measurements were made at a number of positions across the self-preserving wake of a circular cylinder, of diameter $d = 2.67$ mm, at a distance of $420d$ from the cylinder. The mean velocity profile at the measurement station is shown in figure 1. The Reynolds number, based on the free-stream velocity $\bar{U}_{1\infty}$ (= 6.7 m/s) and cylinder diameter d was 1170, while the turbulence Reynolds number $R_\lambda = u_1'\lambda/\nu$, where λ is the longitudinal Taylor microscale, varied from about 40 at the centreline, to about 80 at $x_2^* = 2.0$. The prime denotes a r.m.s. value and the asterisk represents normalization by the local mean velocity $\bar{U}_1$ and/or L, where L is the mean velocity defect half-width. At the measurement station, L is 12.3 mm and the mean velocity defect U_0 (figure 1) is 0.36 m/s. The Kolmogorov microscale $\eta[\equiv (\nu^3/\bar{\epsilon}_1)^{\frac{1}{4}}$, where $\bar{\epsilon}_1$ is the average isotropic turbulent energy dissipation $= 15\nu\overline{u_{1,1}^2}]$ increases from about 0.45 mm at the centreline to about 0.7 mm at $x_2^* \approx 2.0$. Full details of the experimental apparatus and experimental conditions have been given elsewhere (Antonia & Browne 1986; I) and will not be repeated here.

As noted earlier, the components of ω_i were obtained from a number of separate experiments, each involving two parallel X-probes. The components of ω_2 were obtained simultaneously, as were those of ω_3. In the case of the ω_2 components, the X-wires were aligned in the (x_1, x_3)-plane and separated by a distance $\Delta x_3 \approx 1.6$ mm. In the case of the ω_3 components, the X-wires were in the (x_1, x_2)-plane with a separation $\Delta x_2 \approx 1.6$ mm. The two components of ω_1 were obtained separately, the first $(u_{3,2})$ using two X-wires in the (x_1, x_3)-plane separated by a distance $\Delta x_2 \approx 1.6$ mm and the second $(u_{2,3})$ using two X-wires in the (x_1, x_2)-plane separated by a distance $\Delta x_3 \approx 1.6$ mm. The wires in each of the X-probes were 1 mm apart.

The signals from the X-wires were low-pass filtered at a frequency $f_c(-3\,\mathrm{dB})$ approximately equal to the Kolmogorov frequency $f_K(=\bar{U}_1/2\pi\eta)$ and sampled at a frequency equal to $2f_c$ into a PDP 11/34 computer using a 12 bit A/D converter. The record duration was 45 seconds. The choice of $f_c \approx f_K$ was dictated mainly by the onset of noise in the spectra of $u_{1,1}$, $u_{2,1}$, $u_{1,2}$ and $u_{2,2}$ at $f_c \approx 1.1 f_K$. From these signals and the velocity-yaw calibrations of the X-probes, digital time series were constructed for the velocity fluctuations u_i. Digital time series of ω_2 and ω_3 were then formed, using the approximations

$$\omega_2 \approx \frac{\Delta u_1}{\Delta x_3} + \bar{U}_1^{-1}\frac{\Delta u_3}{\Delta t},$$

and

$$\omega_3 \approx -\bar{U}_1^{-1}\frac{\Delta u_2}{\Delta t} - \frac{\Delta u_1}{\Delta x_2},$$

Δu_i is the difference between the u_i signals and Δt is the time interval, equal to the inverse of the sampling frequency, between consecutive samples. Note that $\Delta u_3/\Delta t$ and $\Delta u_2/\Delta t$ were computed from the time series of u_3 and u_2, measured at one of the X-wire locations; the statistics of ω_2 and ω_3 were essentially unchanged when u_3 and u_2 were taken at the other X-wire location. In the calculation of ω_2 and ω_3, the cross-stream resolution length ($\Delta x_2 = \Delta x_3 \approx 1.6$ mm) is approximately the same as the streamwise resolution length ($\bar{U}_1 \Delta t \approx 1.4$ mm).

In order to ascertain that the velocity derivatives involved in the measurement of the vorticity fluctuations were measured reliably with the present two X-probes arrangement, a number of checks were made. One of these checks (see I) consisted of comparing the values of u_1' obtained from each X-probe with those measured with a single hot wire. A more important check, in the present context, was to compare the derivatives $u_{1,2}$ and $u_{1,3}$ as inferred from the two X-probes, with values obtained using two parallel hot wires for the same lateral separation as with the two X-probes. For both $u_{1,2}'$ and $u_{1,3}'$, agreement at several values of x_2^* was found to be better than 5%. No correction to the X-probes was made for the possible effect of $\bar{U}_{1,2}$ since this mean velocity gradient is small in this flow. At $x_2^* \approx 0.8$, where the magnitude of $\bar{U}_{1,2}$ is largest ($L\bar{U}_{1,2}/\bar{U}_{1\infty} \approx 0.04$), the maximum values of $|u_{1,2}|$ and $|u_{1,3}|$ were larger than $\bar{U}_{1,2}$ by factors of 11 and 10 respectively. A consequence of these values of $\bar{U}_{1,2}$ and $u_{1,2}$ is that the two X-probe arrangement is inadequate for resolving the mean velocity gradient but can adequately resolve fluctuating velocity gradients. No corrections have been applied for the effects of the cross-stream velocity components on the X-probes, primarily because the local turbulence levels are quite small in this flow (at the measurement station, the maximum value of $u_1'/\bar{U}_1$ is less than 2%). It should be noted that although the influence of the cross-stream components has been ignored here, this influence could be important in other flows. For example, Wallace & Vukoslavčević (1981) found that in the near-wall region of a turbulent boundary layer, the influence of the instantaneous velocity gradients and cross-stream velocity components cause extremely large errors in the streamwise vorticity component measured with a modified Kovasznay four-wire probe.

Taylor's hypothesis $\partial/\partial x_1 \equiv -\bar{U}_1^{-1}\partial/\partial t$, was used to convert temporal derivatives into derivatives with respect to the streamwise direction. Corrections to Taylor's hypothesis to account for the influence of a fluctuating velocity field were not applied here. A general, though brief, discussion of the conflicting evidence on existing corrections, was given in Antonia, Anselmet & Chambers (1986). It is however worth recalling here that (Browne, Antonia & Rajagopalan 1983) good agreement was found on the centreline of a turbulent plane jet between various statistics of the

actually measured $\partial\theta/\partial x_1$ (θ is the temperature fluctuation) and those obtained by Taylor's hypothesis. This result should be applicable in the present flow where the turbulence levels are much smaller than in the plane jet. It should further be noted that, at $x_1/d = 420$, the maximum mean velocity variation across the wake is about $0.05\bar{U}_{1\infty}$ (figure 1) so that Taylor's hypothesis would also be a reasonable approximation to the large-scale structure.

To provide a measure of the accuracy of the measurement of ω_i, estimates were made at the largest value of x_2^* (≈ 2.0) at which data were taken of r.m.s. values of ω_2 and ω_3 in the non-turbulent flow.

The on–off intermittency function $I(t)$ ($= 1$ in the turbulent region and 0 in the non-turbulent region) was obtained by comparing ω_2^2 or ω_3^2 with a threshold level k. A sufficiently wide range of k was identified for which the average crossing frequency of $I(t)$ was approximately constant; over this range, ω_i' in the turbulent zone and the non-turbulent zones, calculated with respect to the zone averages, were also approximately constant. The ratio $(\omega_i')_{\text{turbulent}}/(\omega_i')_{\text{non-turbulent}}$ was found to be equal to about 11 for $i = 2$ and 10 for $i = 3$; these values represent an estimate of the spurious vorticity measured by the pair of X-probes.

4. Results for the r.m.s., p.d.f., skewness and flatness of ω_i

Distributions, across the wake, of r.m.s. values of the components of ω_i are plotted in the form $\omega_i'^*$ *vs.* x_2^* in figure 2. The values of ω_1' were determined with the approximation

$$\omega_1' \approx (\overline{u_{3,2}^2} + \overline{u_{2,3}^2})^{\frac{1}{2}}, \tag{14}$$

i.e. by assuming that the correlation between $u_{3,2}$ and $u_{2,3}$ is zero.

It is appropriate to discuss the experimental evidence with respect to the above assumption. The correlation coefficients $\overline{u_{3,2}u_{2,3}}/u_{3,2}'u_{2,3}'$, $\overline{u_{2,1}u_{1,2}}/u_{2,1}'u_{1,2}'$ and $\overline{u_{1,3}u_{3,1}}/u_{1,3}'u_{3,1}'$, obtained using the isotropic relation

$$\overline{u_{i,j}u_{k,m}} = \tfrac{1}{2}\overline{u_{1,1}^2}(4\delta_{ik}\delta_{jm} - \delta_{ij}\delta_{km} - \delta_{im}\delta_{jk}), \tag{15}$$

would all be equal to -0.25. The measured coefficients $\overline{u_{2,1}u_{1,2}}/u_{2,1}'u_{1,2}'$ and $\overline{u_{1,3}u_{3,1}}/u_{1,3}'u_{3,1}'$ vary from about -0.06 at the wake centreline to about -0.15 at $x_2^* \approx 2.0$.

It also follows from (15) that the correlation coefficients $\overline{u_{1,1}u_{2,2}}/u_{1,1}'u_{2,2}'$, $\overline{u_{1,1}u_{3,3}}/u_{1,1}'u_{3,3}'$ and $\overline{u_{2,2}u_{3,3}}/u_{2,2}'u_{3,3}'$ should all be equal to -0.5. Measured values of the first two coefficients fall in the range -0.25 ($x_2^* = 0$) to about -0.4 ($x_2^* \approx 2$). The third correlation coefficient could not be measured in the present experiment; we have however estimated it from the continuity equation, expressed in the form†

$$\overline{u_{1,1}^2} = \overline{(u_{2,2} + u_{3,3})^2}$$

and measured values of $\overline{u_{1,1}^2}$, $\overline{u_{2,2}^2}$ and $\overline{u_{3,3}^2}$. The resulting correlation coefficient $\overline{u_{2,2}u_{3,3}}/u_{2,2}'u_{3,3}'$ is about -0.7 independently of x_2^*. Although the magnitude of this coefficient seems large, the departure from isotropy is no larger than that observed for the coefficients $\overline{u_{2,1}u_{1,2}}/u_{2,1}'u_{1,2}'$ and $\overline{u_{1,3}u_{3,1}}/u_{1,3}'u_{3,1}'$.

The above considerations and the discussion in § 5, which relates to the formation of the approximate spectrum of ω_1, tend to suggest that the magnitude of $\overline{u_{3,2}u_{2,3}}/u_{3,2}'u_{2,3}'$ may be slightly larger than that of the correlation coefficients which appear

† Balint *et al.* (1987) use this equation to check Taylor's hypothesis by comparing the right-hand side with $\overline{u_{1,t}^2}/\bar{U}_1^2$.

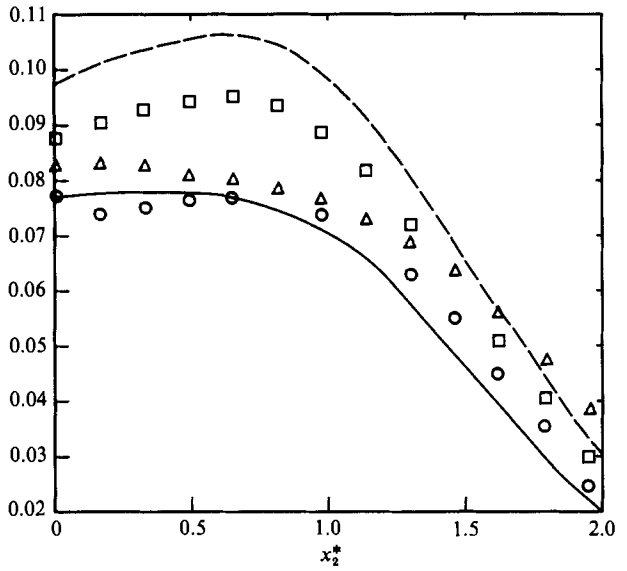

FIGURE 2. Root mean square vorticity components. □, $\omega_1'^*$ using (14); ○, $\omega_2'^*$; △, $\omega_3'^*$; ——, $(5\overline{u_{1,1}^2})^{\frac{1}{2}}L/U_1$; ——, estimate of $\omega_1'^*$ using $\omega_1' = \overline{(u_{3,2}-u_{2,3})^2}^{\frac{1}{2}}$ and the isotropic value for $\overline{u_{3,2}u_{2,3}}$.

in ω_2' and ω_3' and therefore the neglect of the cross-term in (14) is not completely justifiable. A value of about -0.25, i.e. the isotropic value, would seem to be a reasonable estimate for $\overline{u_{3,2}u_{2,3}}/u_{3,2}'u_{2,3}'$.

The results in figure 1 indicate that ω_2' and ω_3' are approximately equal and decrease monotonically with distance from the centreline. By contrast, ω_1' is maximum at $x_2^* \approx 0.7$ and is significantly larger than ω_2' or ω_3' except near the edge of the wake where the intermittency factor ($\equiv \bar{I}$) becomes small (at $x_2^* \approx 1.8$, this factor is approximately 0.25). Estimates of ω_1' obtained with the relation

$$\omega_1' = \overline{(u_{3,2}-u_{2,3})^2}^{\frac{1}{2}}$$

and an assumed isotropic value (-0.25) for the correlation coefficient are also shown in figure 2. These estimates are about 10% larger than those inferred from (14).

The relative behaviour of the distributions in figure 2 can be compared with those obtained by Balint *et al.* (1987) in a boundary layer. The latter authors obtained simultaneous values of $\overline{\omega_1^2}$, $\overline{\omega_2^2}$ and $\overline{\omega_3^2}$ (for this flow, ω_1 is in the longitudinal direction, ω_2 is in the direction normal to the wall and ω_3 is in the spanwise direction) using a miniature nine-sensor hot-wire probe. In the outer part of the logarithmic region and in the wake-like region, $\overline{\omega_2^2}$ and $\overline{\omega_3^2}$ are approximately equal and smaller in magnitude than $\overline{\omega_1^2}$, in a manner similar to that exhibited by the present data (figure 2). Balint *et al.*'s near-wall measurements and those of Kastrinakis & Eckelmann (1983) in a turbulent channel flow indicate that the maximum value of ω_1' occurs near $x_2^+ \approx 20$ (the superscript + representing normalization with wall variables) where the average production of turbulent energy is maximum. The value of x_2^* (≈ 0.7) at which the present distribution of ω_1' is maximum corresponds approximately with the maximum of turbulent energy production.

It follows from (1) and the isotropic relation (15) that $\overline{\omega_1^2}$, $\overline{\omega_2^2}$ and $\overline{\omega_3^2}$ are equal to $5\overline{u_{1,1}^2}$. Figure 2 shows that ω_1' is significantly larger than the isotropic value whereas

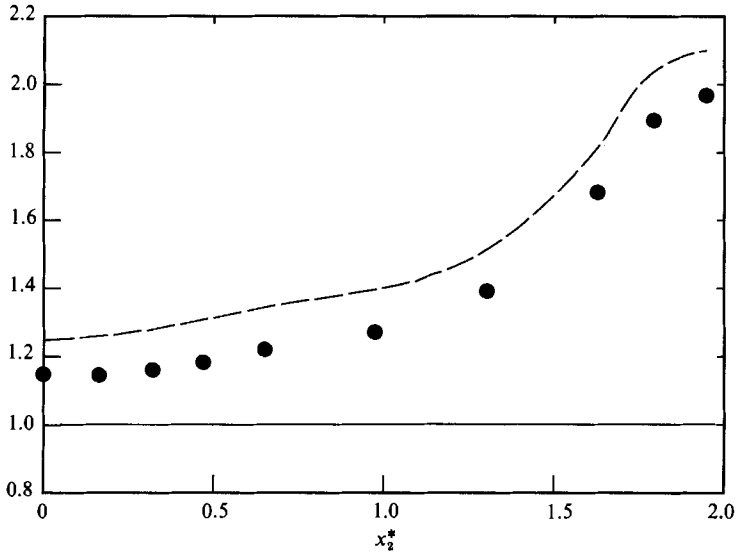

FIGURE 3. Comparison with isotropy of the sum of the mean square values of the vorticity components. ●, $(\overline{\omega_1^2}+\overline{\omega_2^2}+\overline{\omega_3^2})/15\overline{u_{1,1}^2}$; ——, isotropic value, (16); ——, using $\overline{\omega_1^2} = \overline{(u_{3,2}-u_{2,3})^2}$ and the isotropic value for $\overline{u_{3,2}u_{2,3}}$.

ω_2' and ω_3' are in reasonable agreement with the isotropic value in the fully turbulent region. For isotropy, the sum of the components of $\overline{\omega_i^2}$ is given by

$$\overline{\omega_1^2}+\overline{\omega_2^2}+\overline{\omega_3^2} = \frac{\bar{\epsilon}_1}{\nu}. \tag{16}$$

The ratio of the left- and right-hand sides of (16) is plotted in figure 3 and would have a value of 1 if isotropy applied. The departure from isotropy increases slowly away from the centreline. The magnitude of the ratio is about 20% larger than the isotropic value in the fully turbulent part of the wake ($\bar{I} = 0.91$ at $x_2^* \approx 1.0$). The magnitude of this ratio increases by about 10% (figure 3) if the relation $\omega_1' = \overline{(u_{3,2}-u_{2,3})^2}^{\frac{1}{2}}$ is used with the isotropic value for $\overline{u_{3,2}u_{2,3}}$.

The probability density function p of ω_i ($i = 2, 3$) was obtained at several locations in the fully turbulent region. The distributions shown in figure 4 indicate good symmetry but a noticeable departure from the Gaussian distribution for large magnitudes of the fluctuation, the departure increasing as $|\omega_i|$ increases. This departure is obvious even though the oscillations in the measured probability density function increase with the magnitude of ω_2 and ω_3.

Since the skewness $\overline{\omega_i^3}/\omega_i'^3$ and flatness factor $\overline{\omega_i^4}/\omega_i'^4$ provide quantitative measures of the departure of p from a Gaussian distribution, it is of interest to consider the variation of these two quantities across the flow. Balint *et al.* (1987) have noted, using flow symmetry considerations, that the skewnesses of ω_1 and ω_2 should be zero everywhere. In the wall region of a boundary layer, they found that the skewnesses of ω_1 and ω_2 are negligible and attributed the non-zero skewness of ω_3 (typically -1) to spanwise vortex stretching activity. The skewness (figure 5i) of ω_2 is zero throughout the fully turbulent region, the location ($x_2^* \approx 1$) where the departure from zero first occurs corresponding approximately with the start of the intermittent region. The skewness of ω_3 is approximately zero in the fully turbulent region. The difference between this behaviour and that in the boundary layer can perhaps be

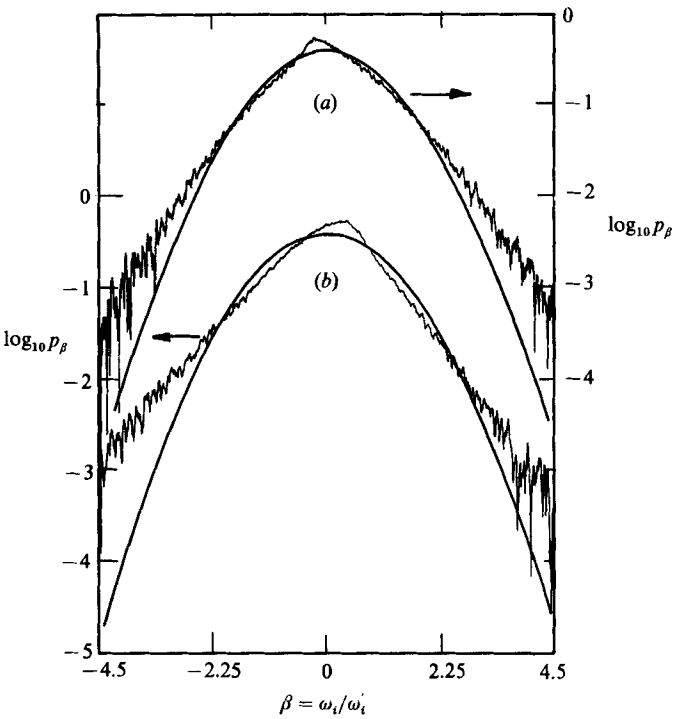

FIGURE 4. Probability density functions of lateral vorticity components at $x_2^* \approx 0.98$. (*a*) $i = 2$; (*b*) $i = 3$. ——, Gaussian.

ascribed to the continuous generation of vorticity associated with the boundary-layer wall. Unfortunately, Balint *et al.* (1987) do not present data for the skewness of ω_i in the 'wake' region of the boundary layer, where comparison with the present data in the intermittent region may have been more relevant.

The flatness factors (figure 5ii) of ω_2 and ω_3 are approximately constant in the range 3.5 to 4, in the fully turbulent region and begin to increase for $x_2^* \gtrsim 1$. Also shown in figure 5 are the skewness and flatness factors of the derivatives that make up the vorticity components. Comparison of the behaviour of the skewness and flatness factors of $u_{2,3}$ and $u_{3,2}$ with those of the corresponding components of ω_2 and ω_3 suggests that the flatness factor of ω_1 may be similar to that of ω_2 or ω_3 while the skewness of ω_1 may increase more slowly, near the edge of the wake, than that of ω_2 or ω_3.

The measurements of Kastrinakis & Eckelmann (1983) in a fully developed turbulent channel flow indicate that the skewness of ω_1 is zero except near the wall while the flatness factor of ω_1 increases away from the wall becoming constant only near the channel centreline. These authors suggested that this increase may indicate that streamwise vortices occur less frequently as the distance from the wall increases. If a similar interpretation is applied to the present data, the distributions of figure 5 would tend to imply a homogeneous distribution of three-dimensional vortices in the fully turbulent flow region. Since the increase in the flatness factor is strictly associated with intermittency, one would expect to find fewer vortices in this region. To gain a clearer picture of the vortical structure of this flow, information is needed on the three-dimensional vorticity associated with the large-scale motion. The flow visualizations in Antonia *et al.* (1987*a*) suggested the presence of clusters of

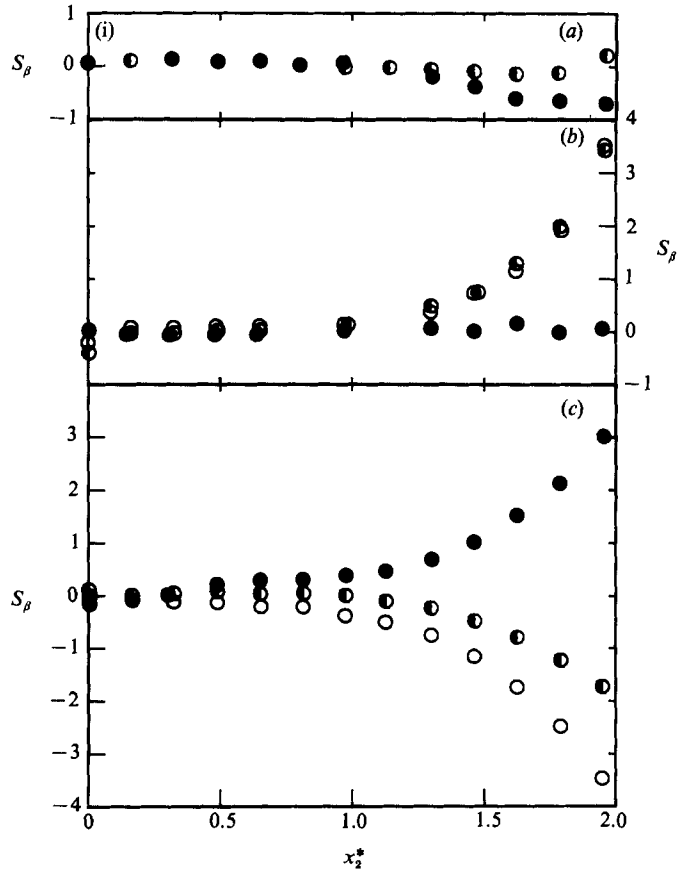

FIGURE 5(i). For caption see facing page.

vortex loops (possibly hairpin vortices). Such a vortex model implies a preferential organization of the large-scale vorticity but would have to be consistent with the fluctuating vorticity statistics presented here.

5. Results for the spectra of ω_i

Spectra of ω_2, ω_3 and of the separate constituents of ω_1 were obtained at several locations across the wake. Although results are shown (figure 6) at only one position ($x_2^* \approx 0.98$), it was ascertained that they are representative of results obtained at smaller and larger x_2^* ($0 \lesssim x_2^* \lesssim 2.0$)†. Spectra of ω_i or of $u_{i,j}$ are normalized so that

$$\int_0^\infty 2\phi_\beta(k_1\eta)\,\mathrm{d}(k_1\eta) = \overline{\beta^2}\frac{\eta^2}{U_K^2}, \tag{17}$$

where β stands for either ω_i or $u_{i,j}$, $U_K\,[\equiv(\nu\bar{\epsilon}_I)^{\frac{1}{4}}]$ is the Kolmogorov velocity, $k_1 = 2\pi f/\bar{U}_1$ and the factor of 2 has been included for consistency with the definition of ϕ_{ω_i} given in relation (7). The maximum value of the ratio l_w/η was 2.7 (at the

† The location $x_2^* \approx 0.98$ lies at approximately the edge of the fully turbulent region since $\bar{I}$ is approximately 0.92 there. Also, the flow topology obtained by Browne, Antonia & Bisset (1986) indicated that coherent structures are centred at $x_2^* \approx 1$.

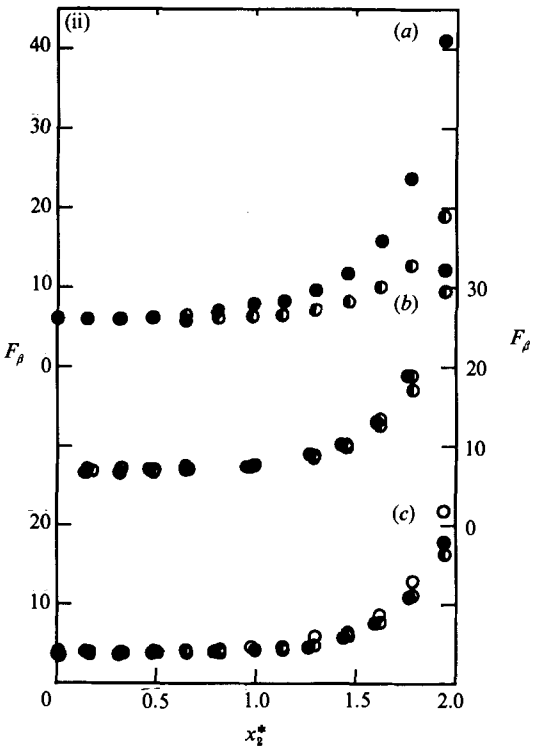

FIGURE 5. Skewness and flatness factors of vorticity components and of velocity derivatives that make up the vorticity. (i) Skewness S_β: (*a*) ◐, $\beta = u_{3,2}$; ●, $u_{2,3}$. (*b*) ○, ω_2; ◐, $u_{1,3}$; ●, $u_{3,1}$. (*c*) ○, ω_3; ◐, $u_{2,1}$; ●, $u_{1,2}$. (ii) Flatness factor F_β: symbols same as in (i).

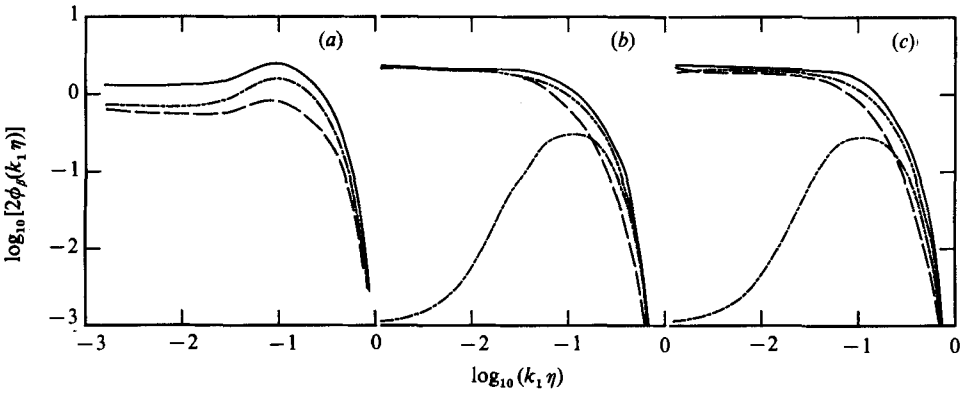

FIGURE 6. Spectra of vorticity components and their associated velocity derivatives. (*a*) ω_1: ——, $\phi_{\omega_1} \approx \phi_{u_{2,3}} + \phi_{u_{3,2}}$; — — —, $\phi_{u_{2,3}}$; — — — —, $\phi_{u_{3,2}}$. (*b*) ω_2: ——, ϕ_{ω_2}; — — —, $\phi_{u_{1,3}}$; — — — —, $\phi_{u_{3,1}}$; — · — · —, $\phi_{u_{1,3}} + \phi_{u_{3,1}}$. (*c*) ω_3: ——, ϕ_{ω_3}; — — —, $\phi_{u_{1,2}}$; — — — —, $\phi_{u_{2,1}}$; — · — · —, $\phi_{u_{1,2}} + \phi_{u_{2,1}}$.

wake centreline) and the hot-wire length corrections of Wyngaard (1968) indicate that the attenuation in the measured one-dimensional spectrum, which increases as the wavenumber increases, is about 14% at $k_1\eta \approx 0.9$. Since this correction is of the same order as the experimental uncertainty, wire length corrections were not applied to ϕ_β. Corrections were however applied for the effect of lateral separation between the X-probes on the spectra of $u_{i,j}$ when j is equal to 2 or 3. The correction procedure adopted was similar to that outlined by Wyngaard (1969) for the case of parallel hot

wires, except for the choice (see Appendix) of the three-dimensional spectrum $E(k)$. Corrections were made by multiplying the measured spectra of $u_{i,j}$ ($j = 2$ or 3), obtained for a finite separation Δx_j between the X-wires, with the ratio

$$\phi_{u_{i,j}}(\Delta x_j = 0, k_1)/\phi_{u_{i,j}}(\Delta x_j, k_1)$$

where

$$\phi_{u_{i,j}}(\Delta x_j, k_1) = \frac{4}{(\Delta x_j)^2}\int\int_{-\infty}^{\infty} \sin^2 \tfrac{1}{2}(k_j \Delta x_j)\, \phi_{ii}(\boldsymbol{k})\, \mathrm{d}k_2\, \mathrm{d}k_3.$$

Using isotropy, the above double integral can be directly evaluated with the use of relation (11) and expression (A 2) for $E(k)$. For $\Delta x_j/\eta \approx 3.2$, the ratio

$$\phi_{u_{i,j}}(\Delta x_j = 0, k_1)/\phi_{u_{i,j}}(\Delta x_j, k_1)$$

typically increased from about 1.1 at $k_1\eta \approx 0.1$ to about 1.5 at $k_1\eta \approx 0.9$.

The spectrum of ω_i receives contributions from the spectra and cospectra of the constituent velocity derivatives. For example, in the case of ω_3, the time autocorrelation $\overline{\omega_3(t)\,\omega_3(t+\tau)}$ can be expressed as

$$\overline{\omega_3(t)\,\omega_3(t+\tau)} = \overline{u_{2,1}(t)\,u_{2,1}(t+\tau)} + \overline{u_{1,2}(t)\,u_{1,2}(t+\tau)} - \overline{u_{2,1}(t)\,u_{1,2}(t+\tau)} - \overline{u_{1,2}(t)\,u_{2,1}(t+\tau)},$$

and by Fourier transformation,

$$\phi_{\omega_3}(f) = \phi_{u_{2,1}}(f) + \phi_{u_{1,2}}(f) - Co_{u_{2,1}u_{1,2}}(f) - Co_{u_{1,2}u_{2,1}}(f), \tag{18}$$

where Co is the cospectrum. Measurements indicated that the cross correlation of $u_{2,1}$ and $u_{1,2}$ was reasonably symmetric about $\tau = 0$ so that (18) reduces to

$$\phi_{\omega_3}(f) = \phi_{u_{2,1}}(f) + \phi_{u_{1,2}}(f) - 2Co_{u_{2,1}u_{1,2}}(f). \tag{19}$$

The first two terms on the right-hand side of (19) are plotted in figure 6(*c*) as a function of $\log_{10} k_1\eta$†. Also plotted are the sum of these two terms and the sum of all terms on the right-hand side of (19). It is evident that $\phi_{u_{1,2}}$ makes the major contribution to ϕ_{ω_3} for small wavenumbers whereas $\phi_{u_{2,1}}$ becomes more important than $\phi_{u_{1,2}}$ at the larger wavenumbers ($\log_{10} k_1\eta \gtrsim -0.6$). It is also clear that the contribution from the cospectrum is negligible except perhaps over a frequency band for which the spectrum of $u_{2,1}$ is largest. The cospectrum, plotted using a larger scale in figure 7(*b*), is negative everywhere and exhibits a peak near $k_1\eta \approx 0.06$ or $fL/\bar{U}_1 \approx 0.24$ which corresponds approximately to the average frequency of coherent structures in the wake (Antonia, Browne & Fulachier 1987*b*).

The distributions (figure 6*b*) for ϕ_{ω_2} and its constituents are similar to those of figure 6(*c*), the major difference being the even smaller contribution to ϕ_{ω_2} from the cospectrum $Co_{u_{1,3}u_{3,1}}$. Although the latter quantity also exhibits a peak at the average frequency of the structures, it becomes positive for $k_1\eta \gtrsim 0.2$. The magnitude of the peak is comparable to that for $Co_{u_{2,1}u_{1,2}}$ but the change of sign (figure 7*a*) in the cospectrum results in $\overline{u_{1,3}u_{3,1}}$ being slightly smaller than $\overline{u_{1,2}u_{2,1}}$.

The spectra of $u_{2,3}$ and $u_{3,2}$, shown in figure 6(*a*), have qualitatively the same behaviour, each exhibiting a significant peak near the average frequency of structures. It is therefore possible that the cospectrum $Co_{u_{2,3}u_{3,2}}$ may be more important, in terms of its contribution to ϕ_{ω_1}, than the corresponding cospectra of ϕ_{ω_2} and ϕ_{ω_3}. For the purpose of comparing ϕ_{ω_1} with the isotropic calculation (§6), we have assumed that

$$\phi_{\omega_1} \approx \phi_{u_{2,3}} + \phi_{u_{3,2}}, \tag{20}$$

† For convenience, only smooth spectral curves are shown in figure 6. Unsmoothed curves are shown in figures 7, 8 and 9.

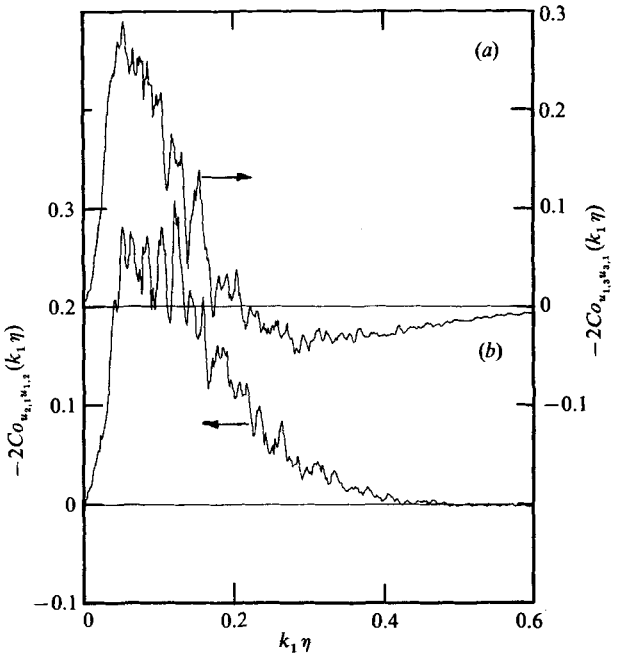

FIGURE 7. Cospectra of velocity derivatives which appear in ω_2 and ω_3. (*a*) $Co_{u_{1,3}u_{3,1}}$; (*b*) $Co_{u_{2,1}u_{1,2}}$.

realizing that it may be in error in a range of frequencies near the average frequency of the structures. The shape of the sum of $\phi_{u_{2,3}}$ and $\phi_{u_{3,2}}$, shown in figure 6(*a*), is quite different from that of ϕ_{ω_2} or ϕ_{ω_3}.

6. Comparison between measured and calculated spectra

The shapes and magnitudes of ϕ_{ω_2} and ϕ_{ω_3}, figures 8(*b*) and 8(*c*), are nearly identical over the full wavenumber range, in apparent agreement with the requirement of isotropy, viz. $\phi_{\omega_2}(k_1) = \phi_{\omega_3}(k_1)$, and in agreement with the comments made in discussing figure 2. Isotropic calculations for the ω_2 and ω_3 spectra were obtained by carrying out the integration in (12) using an expression for $E(k)$, details of which are given in the Appendix. The measured spectrum of ω_2 is in reasonable agreement with the calculation for $k_1\eta \gtrsim 0.4\,(\equiv \log_{10} k_1\eta \gtrsim -0.4)$. Similarly the measured spectrum of ω_3 is in reasonable agreement with the calculation for

$$k_1\eta \gtrsim 0.55\,(\equiv \log_{10} k_1\eta \gtrsim -0.26).$$

For $k_1\eta \gtrsim 0.7$, the calculation is slightly larger than the measurement, the difference tending to increase with $k_1\eta$. It should be noted here that the corrections which have been made to the measured spectra of ω_2 and ω_3 correspond identically to corrections made to spectra of $u_{1,3}$ and $u_{1,2}$ respectively for the effects of finite separations Δx_3 and Δx_2, i.e. no corrections were made for the spectra involving streamwise derivatives. It is unlikely that spectral corrections resulting from the assumption of Taylor's hypothesis are significant. More likely reasons for the discrepancy are an insufficiency of the corrections for the separation Δx_j and the lack of perfect agreement (see Appendix) between isotropy and the measured spectra of u_1, u_2 and u_3.

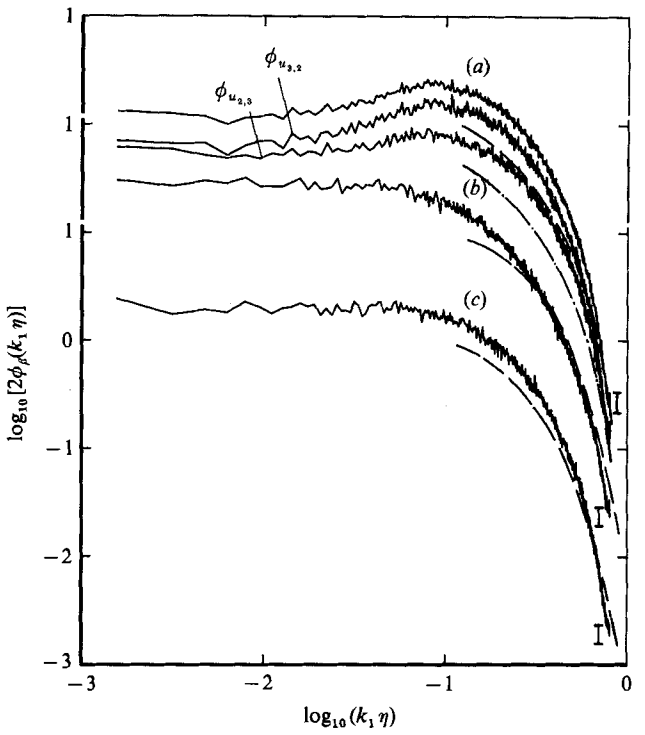

FIGURE 8. Comparison between measured spectra and isotropic calculations. (*a*) ——, measured $\phi_{u_{3,2}}$ and approximated ϕ_{ω_1} using (20); — —, calculated ϕ_{ω_1} using (13) and (A2); — · —, calculated $\phi_{u_{2,3}}$ or $\phi_{u_{3,2}}$ using (21) and (A2). (*b*) ——, measured ϕ_{ω_2}; — —, calculated ϕ_{ω_2} using (12) and (A2). (*c*) ——, measured ϕ_{ω_3}; — —, calculated ϕ_{ω_3} using (12) and (A2). Vertical bars (I) indicate maximum experimental uncertainty in measured vorticity spectra at $k_1\eta \approx 0.83$.

Since ω_1 has not been measured, it is difficult to draw firm conclusions from the comparison between the calculated distribution of ϕ_{ω_1}, obtained using (13) and (A 2) and the measured approximation to ϕ_{ω_1}. There is no reason, however, to suspect the convergence between calculation and measurement at very large wavenumbers since the contribution from the neglected cross spectrum in (20) should be negigible at those wavenumbers. Support for the latter assertion was provided by the excellent agreement obtained, for $k_1\eta > 0.25$, between the spectrum of ω_1, calculated using (13) and (A 2), and the sum of the calculated spectra of $u_{2,3}$ and $u_{3,2}$. The isotropic calculation for $\phi_{u_{2,3}}$ or $\phi_{u_{3,2}}$, viz.

$$\phi_{u_{2,3}}(k_1) = \phi_{u_{3,2}}(k_1) = \int_{k_1}^{\infty} \frac{E(k)}{4}\left(1-\frac{k_1^2}{k^2}\right)k\,\mathrm{d}k - \int_{k_1}^{\infty} \frac{E(k)}{16}\left(1-\frac{k_1^2}{k^2}\right)^2 k\,\mathrm{d}k, \qquad (21)$$

was obtained using a procedure similar to that outlined in Antonia, Browne & Chambers (1984) for $\phi_{u_{1,2}}$ or $\phi_{u_{1,3}}$.

Agreement between the measured spectrum of $u_{2,3}$ or $u_{3,2}$ and the calculation, using (21) and (A 2), occurs only for very large wavenumbers (figure 8*a*). Consequently, the agreement between the measured approximation to ϕ_{ω_1} and the calculated distribution of ϕ_{ω_1}, obtained with (13) and (A 2), extends only over this range of wavenumbers (figure 8*a*). The relative behaviour of measured and calculated spectra in figure 8(*a*) is consistent with the departure from isotropy of ω_1' (figure 2). Wallace (1986) noted that the one-dimensional vorticity spectrum of ω_1, measured by

Kistler (1952) in a turbulent grid flow, was in agreement, at high wavenumbers, with the spectrum calculated using ϕ_{u_1} but diverged considerably from the calculation at low wavenumbers.

The apparently slower approach to local isotropy by ω_1 than by ω_2 or ω_3 requires an explanation. The spectrum of u_2, and to a lesser extent that of u_3, reflects the imprint of the organized large-scale motion, exhibiting a significant peak at the average frequency of this motion (e.g. Cimbala 1985; Antonia *et al.* 1987*b*). The spectrum of u_1 exhibits no such peak, so it is conceivable that u_1 is less affected than either u_2 or u_3 by the anisotropy of the large-scale motion. In this context, it is plausible that ω_1 which contains information about both u_2 and u_3 is more influenced by the large-scale motion than ω_2 or ω_3, the latter including information about u_1 as well as u_2 or u_3. It should of course, be added that as the Reynolds number increases, the ratio of the peak frequency in the u_2 or u_3 spectrum to the Kolmogorov frequency will decrease so that the anisotropy of the large-scale motion should have less effect on ω_2, ω_3 and more on ω_1.

7. Conclusions

The measurements indicate approximately the same behaviour across the wake for the moments and spectra of the lateral components of vorticity. Although statistics of the longitudinal component of vorticity have been inferred indirectly from the statistics of individual velocity derivatives, there is sufficient evidence to suggest that the statistics of ω_1 differ from those of ω_2 or ω_3. Mean square values of ω_i deviate from local isotropy, but the deviation is less pronounced for ω_2 or ω_3 than for the approximation to ω_1.

Over a significant high-wavenumber range, measured spectra of ω_2 and ω_3 are in satisfactory agreement with the calculation, in reasonable support of local isotropy. By contrast, agreement with isotropy of the approximation to the longitudinal vorticity spectrum is approached only at very large wavenumbers. It is possible that the components of ω_1 feel the anisotropy of the large-scale motion more directly than the components of ω_2 or ω_3.

The present statistics of ω_2 and ω_3 should provide a useful point of reference when simultaneous measurements of the three components of vorticity are made with a fixed geometry multiple-wire probe. Such a probe is currently being constructed in our laboratory and it is planned to use it in the same flow to gain more insight into the organized vortical structure of this flow.

The support of the Australian Research Grants Scheme is gratefully acknowledged.

Appendix. Choice of the three-dimensional energy spectrum

To evaluate the integrals in (12), (13) and (21), an expression for $E(k)$ is required. There are several ways of arriving at such an expression. One way would be to select $E(k)$ so that it satisfies the measured spectrum of u_1 at large wavenumbers, the isotropic relation between $E(k)$ and $\phi_{u_1}(k_1)$ being given by

$$E(k) = k^2\left(\frac{\mathrm{d}^2\phi_{u_1}}{\mathrm{d}k_1^2}\right)_{k_1=k} - k\left(\frac{\mathrm{d}\phi_{u_1}}{\mathrm{d}k_1}\right)_{k_1=k}$$

The resulting form of $E(k)$ should strictly satisfy the measured spectra of u_2 and u_3 at large wavenumbers, provided local isotropy is valid. For $k_1\eta \gtrsim 0.15$, the

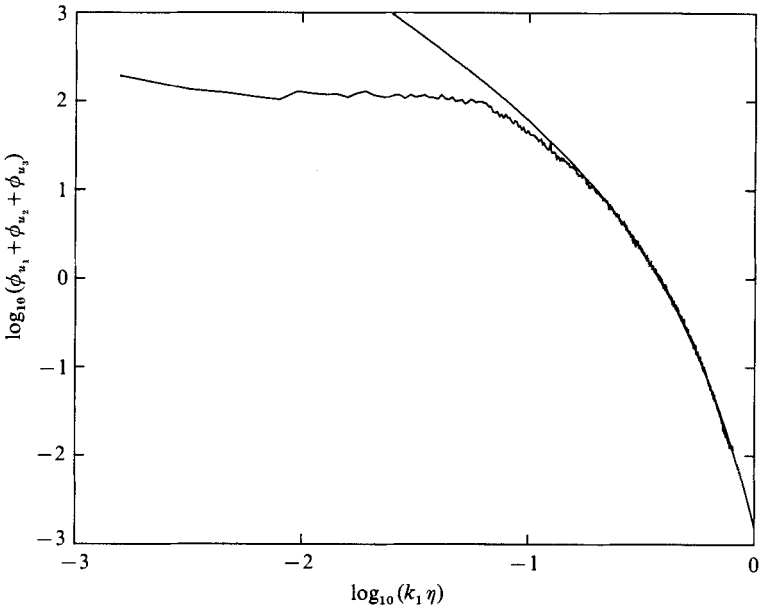

FIGURE 9. Comparison of the measured one-dimensional energy spectrum with the calculation based on a particular choice of $E(k)$. ——, calculated with (A 1) and (A 2) with $\alpha_1 = 3.85, \alpha_2 = 3.67$.

agreement between the measured spectra of u_1, u_2, u_3 and isotropy was reasonable but not perfect. It seemed therefore appropriate to select $E(k)$ in order to satisfy the measured spectra collectively rather than to base the selection on the spectrum of a particular velocity component. $E(k)$ was chosen to satisfy the one-dimensional energy spectrum, i.e. the sum of the spectra of u_1, u_2, u_3, viz.

$$\phi_{u_1}(k_1)+\phi_{u_2}(k_1)+\phi_{u_3}(k_1) = \int_{k_1}^{\infty} \frac{E(k)}{k}\,\mathrm{d}k. \tag{A 1}$$

$E(k)$ was assumed to be represented by the expression

$$E(k) = \alpha_1 \bar{\epsilon}^{\frac{2}{3}} k^{-\frac{5}{3}} \exp\left[-\tfrac{3}{2}\alpha_2 (k\eta)^{\frac{4}{3}}\right], \tag{A 2}$$

and the constants α_1 and α_2 were varied to provide the best fit to (A 1) at large enough values of k_1. Figure 9 indicates that good agreement with the one-dimensional energy spectrum is obtained for $k_1\eta \gtrsim 0.15 (\equiv \log_{10} k_1\eta \gtrsim -0.82)$ with $\alpha_1 = 3.85$ and $\alpha_2 = 3.67$. Relation (A 2) was used, with these values of α_1 and α_2, to estimate ϕ_{ω_t} and $\phi_{u_{2,3}}$ or $\phi_{u_{3,2}}$.

When $\alpha_1 = \alpha_2 = \alpha$, relation (A 2) reduces to the expression derived by Corrsin (1964) and Pao (1965). Wyngaard (1968, 1969) used the Corrsin–Pao form for $E(k)$, with $\alpha = 1.7$, to estimate corrections due to wire length and wire separation. It would however be difficult to justify a universal value of α or indeed a universal form of $E(k)$; here, no special significance is attributed to $E(k)$ beyond its empirical usefulness.

REFERENCES

ANTONIA, R. A., ANSELMET, F. & CHAMBERS, A. J. 1986 Assessment of local isotropy using measurements in a turbulent plane jet. *J. Fluid Mech.* **163**, 365–391.

ANTONIA, R. A. & BROWNE, L. W. B. 1986 Anisotropy of the temperature dissipation in a turbulent wake. *J. Fluid Mech.* **163**, 393–403.

ANTONIA, R. A., BROWNE, L. W. B., BISSET, D. K. & FULACHIER, L. 1987*a* A description of the organized motion in the turbulent far-wake of a cylinder at low Reynolds number. *J. Fluid Mech.* **184**, 423–444.

ANTONIA, R. A., BROWNE, L. W. B. & CHAMBERS, A. J. 1984 On the spectrum of the transverse derivative of the streamwise velocity in a turbulent flow. *Phys. Fluids* **27**, 2628–2631.

ANTONIA, R. A., BROWNE, L. W. B. & FULACHIER, L. 1987*b* Average wavelength of organised structures in the turbulent far wake of a cylinder. *Expts Fluids* **5**, 298–304.

BALINT, J. L., VUKOSLAVČEVIĆ, P. & WALLACE, J. M. 1987 A study of the vortical structure of the turbulent boundary layer. In G. Comte-Bellot & J. Mathieu (ed.), *Advances in Turbulence*, pp. 456–464. Berlin.

BATCHELOR, G. K. 1953 *The Theory of Homogeneous Turbulence.* Cambridge University Press.

BROWNE, L. W. B., ANTONIA, R. A. & BISSET, D. K. 1986 Coherent structures in the far field of a turbulent wake. *Phys. Fluids* **29**, 3612–3617.

BROWNE, L. W. B., ANTONIA, R. A. & RAJAGOPALAN, S. 1983 The spatial derivative of temperature in a turbulent flow and Taylor's hypothesis. *Phys. Fluids* **26**, 1222–1227.

BROWNE, L. W. B., ANTONIA, R. A. & SHAH, D. A. 1987 Turbulent energy dissipation in a wake. *J. Fluid Mech.* **179**, 307–326.

CIMBALA, J. M. 1985 An experimental study of large structures in the far wakes of two-dimensional bluff bodies. *Proc. Fifth Symp. on Turbulent Shear Flows, Cornell University, New York*, pp. 4.1–4.6.

CORRSIN, S. 1964 Further generalization of Onsager's cascade model for turbulent spectra. *Phys. Fluids* **7**, 1156–1159.

CORRSIN, S. & KISTLER, A. L. 1955 Free stream boundaries of turbulent flow. *NACA Rep.* 1244.

ECKELMANN, H., NYCHAS, S. G., BRODKEY, R. S. & WALLACE, J. M. 1977 Vorticity and turbulence production in pattern recognised turbulent flow structures. *Phys. Fluids* **20**, S225–S231.

FOSS, J. F. 1979 Transverse vorticity measurements. In B. W. Hansen (ed.), *Proc. of The Dynamic Flow Conference 1978, Skovlunde*, pp. 983–1001.

KASTRINAKIS, E. G. & ECKELMANN, H. 1983 Measurement of streamwise vorticity fluctuations in a turbulent channel flow. *J. Fluid Mech.* **137**, 165–186.

KISTLER, A. L. 1952 The vorticity meter. MS thesis, Johns Hopkins University.

KOVASZNAY, L. S. G. 1950 *Q. Prog. Rep. of Aero. Dept.* Contract NORD-8036-JHB-39. The Johns Hopkins University.

KOVASZNAY, L. S. G. 1955 Turbulence measurements. In *Physical Measurements in Gas Dynamics and Combustion*, p. 227. Oxford University Press.

PAO, Y. H. 1965 Structure of turbulent velocity and scalar fields at large wavenumbers. *Phys. Fluids* **8**, 1063–1075.

VAN ATTA, C. W. 1979 Multi-channel measurements and high-order statistics. In B. W. Hansen (ed.), *Proc. of The Dynamic Flow Conference 1978, Skovlunde*, pp. 919–941.

VUKOSLAVČEVIĆ, P. & WALLACE, J. M. 1981 Influence of velocity gradients on measurements of velocity and streamwise vorticity with hot-wire X-array probes. *Rev. Sci. Instrum.* **52**, 869–879.

WALLACE, J. M. 1986 Methods of measuring vorticity in turbulent flows. *Expts Fluids* **4**, 61–71.

WALLACE, J. M. & VUKOSLAVČEVIĆ, P. 1982 Measurement of the structure of the streamwise vorticity field in a turbulent boundary layer. In Z. P. Zaric (ed.), *Structure of Turbulence in Heat and Mass Transfer*, pp. 29–42. Hemisphere.

WILLMARTH, W. W. 1979 Nonsteady vorticity measurements: survey and new results. In B. W. Hansen (ed.), *Proc. of The Dynamic Flow Conference 1978, Skovlunde*, pp. 1003–1012.

WYNGAARD, J. C. 1968 Measurement of small scale turbulence structure with hot wires. *J. Phys.* E: *Sci. Instrum.* **1**, 1105–1108.

WYNGAARD, J. C. 1969 Spatial resolution of the vorticity meter and other hot-wire arrays. *J. Phys.* E: *Sci. Instrum.* **2**, 983–987.